

Selection and photometric properties of K+A galaxies

Alejandro D. Quintero¹, David W. Hogg^{1,2}, Michael R. Blanton¹, David J. Schlegel³, Daniel J. Eisenstein⁴, James E. Gunn³, J. Brinkmann⁵, Masataka Fukugita⁶, Karl Glazebrook⁷, and Tomotsugu Goto^{6,8}

ABSTRACT

Two different simple measurements of galaxy star formation rate with different timescales are compared empirically on 156,395 fiber spectra of galaxies with $r < 17.77$ mag taken from the Sloan Digital Sky Survey in the redshift range $0.05 < z < 0.20$: a ratio A/K found by fitting a linear sum of an average old stellar population spectrum (K) and average A-star spectrum (A) to the galaxy spectrum, and the equivalent width (EW) of the $H\alpha$ emission line. The two measures are strongly correlated, but there is a small clearly separated population of outliers from the median correlation that display excess A/K relative to $H\alpha$ EW. These “K+A” (or “E+A”) galaxies must have dramatically decreased their star-formation rates over the last ~ 1 Gyr. The K+A luminosity distribution is very similar to that of the total galaxy population. The K+A population appears to be bulge-dominated, but bluer and higher surface-brightness than normal bulge-dominated galaxies; it appears that K+A galaxies will fade with time into normal bulge-dominated galaxies. The inferred rate density for K+A galaxy formation is $\sim 10^{-4} h^3 \text{ Mpc}^{-3} \text{ Gyr}^{-1}$ at redshift $z \sim 0.1$. These events are taking place in the field; K+A galaxies don’t primarily lie in the high-density environments or clusters typical of bulge-dominated populations.

¹ Center for Cosmology and Particle Physics, Department of Physics, New York University, 4 Washington Place, New York, NY 10003

² To whom correspondence should be addressed: david.hogg@nyu.edu

³ Princeton University Observatory, Princeton, NJ 08544

⁴ Steward Observatory, 933 N. Cherry Ave., Tucson, AZ 85721

⁵ Apache Point Observatory, 2001 Apache Point Road, P.O. Box 59, Sunspot, NM 88349

⁶ Institute for Cosmic Ray Research, University of Tokyo, Kashiwa, 2778582, Japan

⁷ Department of Physics and Astronomy, The Johns Hopkins University, Baltimore, MD 21218

⁸ Department of Physics, Carnegie Mellon University, 5000 Forbes Avenue, Pittsburgh, PA 15213

Subject headings: galaxies: clusters: general — galaxies: evolution — galaxies: fundamental parameters — galaxies: statistics — galaxies: stellar content — stars: formation

1. Introduction

Cosmic star formation activity appears to be coming to an end. All indicators of star formation show that the cosmic mean comoving density of star formation has been declining since redshifts near unity (e.g., Hogg 2001, and references therein). The bulk of stars in the local Universe are found in old stellar populations (Fukugita et al. 1998; Hogg et al. 2002). One consequence of this global decline is that galaxies in the local Universe ought to be shutting down their individual star formation activities. It is not understood whether the changes in star formation in individual galaxies are expected to be gradual or dramatic.

Our extremely local neighborhood in the disk of the Milky Way has been forming stars at a relatively constant rate for the last few billion years (Barry 1988; Pardi & Ferrini 1994; Prantzos & Silk 1998; Rocha-Pinto et al. 2000; Gizis et al. 2002), but it appears that it can't continue for much longer. When the total available gas content is compared to the star formation rate, it appears that the Milky Way will run out of gas in the next few Gyr (e.g., Mooney & Solomon 1988; Blitz 1996). This is also true for the majority of local disk galaxies (Kennicutt et al. 1994). In detail these calculations do not account for gas recycling, gas flux from plasma reservoirs, or new gas accretion, but the trend they imply for cosmic star formation activity is consistent with that found in cosmological observations.

Here we begin a comparison of different optical star-formation rate measurements in a large sample of galaxies with spectroscopic observations in the Sloan Digital Sky Survey (SDSS; e.g., York et al. 2000). One star-formation rate measurement makes use of the strength of the H α emission line, which is emitted in ionization regions around O and B stars, with lifetimes of $\sim 10^7$ yr. Another uses the fraction of the galaxy light emitted by A stars, with lifetimes of $\sim 10^9$ yr. These star-formation indicators are sensitive to stars of different masses and lifetimes.

Star-formation indicators tracking stars with different lifetimes can be compared to flag galaxies with strong star-formation rate derivatives. In particular, comparison of our H α and A-star measurements locates galaxies that have changed their star-formation rates within the last $\sim 10^9$ yr. If star formation is triggered by mergers or interactions, such galaxies might be found to be undergoing or recovering from an interaction, and their statistics

might provide a measure of the merger rate. If star-formation efficiency is a strong function of local environment, then galaxies with negative star-formation derivatives might be tracers of the environmental conditions at the transition between those that are conducive to star-formation and those that aren't.

One population of galaxies with strong negative star-formation rate derivatives is already known: “K+A” or “E+A” galaxies (Dressler & Gunn 1983; Zabludoff et al. 1996; Goto et al. 2003). These are galaxies combining the stellar absorption lines of A stars with those of old stellar populations, but, at the same time, showing little sign of current star-formation. K+A galaxies are exceedingly rare—they comprise between 10^{-2} and $\sim 10^{-4}$ of the galaxy population (depending on definition)—but they are expected to provide important information about the conditions under which stars form and galaxies evolve.

For example, if it is true that elliptical or bulge-dominated galaxies are formed by the mergers of spiral or disk-dominated galaxies, then the central concentration of stars, the alpha-enhanced chemical abundances (e.g., Worthey 1998), and the lack of cold gas, dust and star formation (e.g., Roberts & Haynes 1994) all require large, brief, centrally concentrated starbursts during or immediately following disk–disk mergers. Note that the abundance ratios provide the evidence that the starbursts must be brief. These merger events therefore likely go through a K+A phase for $\sim 10^9$ yr; in this scenario, it should be possible to use the abundances of K+A galaxies to constrain merger rates. Indeed, it has already been shown that the A stars tend to be centrally concentrated in K+A galaxies and that some have “kinematically hot” stellar populations like bulge-dominated galaxies (Norton et al. 2001). On the other hand, in some K+A galaxies, there is residual gas, implying that the star formation event does not always exhaust the entire gas reservoir (Chang et al. 2001).

Although any scenario in which bulge-dominated galaxies are created by mergers virtually requires the remnants to be K+A events, an apparent excess of A stars over O and B stars can be produced in heavily dust-enshrouded star-formation regions from which young stars escape on Gyr timescales, or in mergers in which an old galaxy captures a smaller, younger galaxy, shutting off star formation in the process.

In what follows, a cosmological world model with $(\Omega_M, \Omega_\Lambda) = (0.3, 0.7)$ is adopted, and the Hubble constant is parameterized $H_0 = 100 h \text{ km s}^{-1} \text{ Mpc}^{-1}$, for the purposes of calculating distances and volumes (e.g., Hogg 1999).

2. Data

The SDSS is taking *ugriz* CCD imaging of 10^4 deg 2 of the Northern Galactic sky, and, from that imaging, selecting 10^6 targets for spectroscopy, most of them galaxies with $r < 17.77$ mag (e.g., Gunn et al. 1998; York et al. 2000; Stoughton et al. 2002).

All the data processing, including astrometry (Pier et al. 2003), source identification, deblending and photometry (Lupton et al. 2001), calibration (Fukugita et al. 1996; Smith et al. 2002), spectroscopic target selection (Eisenstein et al. 2001; Strauss et al. 2002; Richards et al. 2002), and spectroscopic fiber placement (Blanton et al. 2003) are performed with automated SDSS software.

Every spectral “plate” of fiber positions includes several faint (15.5 to 18.5 mag) F stars. The spectra are calibrated with these F-star spectra; ie, they are multiplied by the function of wavelength that makes the F-star spectra match F-star spectrophotometry. Although this calibration procedure produces consistent calibration at the 10-percent level (as measured by comparisons of old stellar populations at various redshifts, Eisenstein et al. 2003), it does not deal carefully with the diversity of F-star spectra, or the possibility that some of the F stars, even at inferred distances > 2 kpc, may be inside some part of the Galactic extinction. Inasmuch as the calibration stars are beyond the Galactic extinction, however, the spectra are effectively extinction-corrected.

Redshifts are measured on the reduced spectra by an automated system, which models each galaxy spectrum as a linear combination of stellar eigenspectra (Schlegel, in preparation). The eigenspectra are constructed over the rest-frame wavelength range $4100 < \lambda < 6800$ Å from a high-resolution spectroscopic library (Prugniel & Soubiran 2001). The central velocity dispersion σ_v is determined by fitting the detailed spectral shape as a velocity-smoothed sum of stellar spectra (Schlegel & Finkbeiner, in preparation).

It must be emphasized that the 3 arcsec diameter spectroscopic fibers of the SDSS spectrographs do not obtain all of each galaxy’s light because at redshifts of $0.05 < z < 0.2$ they represent apertures of between 2 and 7 h^{-1} kpc diameter. For this reason, in what follows, SDSS imaging data rather than spectroscopy are used to infer the global properties of the galaxies.

Galaxy luminosities and colors are computed in fixed bandpasses, using Galactic extinction corrections (Schlegel et al. 1998) and K corrections (computed with `kcorrect v1_11`; Blanton et al. 2003). They are K corrected not to the redshift $z = 0$ observed bandpasses but to bluer bandpasses $^{0.1}g$, $^{0.1}r$ and $^{0.1}i$ “made” by shifting the SDSS g , r , and i bandpasses to shorter wavelengths by a factor of 1.1 (c.f., Blanton et al. 2003,a). This means that galaxies at redshift $z = 0.1$ (typical of the sample used here) have trivial K corrections.

To the azimuthally averaged radial profile of every galaxy in the observed-frame i band, a seeing-convolved Sérsic model is fit, as described elsewhere (Blanton et al. 2003a). The Sérsic model has surface brightness I related to angular radius r by $I \propto \exp[-(r/r_0)^{(1/n)}]$, so the parameter n (Sérsic index) is a measure of radial concentration (seeing-corrected). At $n = 1$ the profile is exponential, and at $n = 4$ the profile is de Vaucouleurs.

To every best-fit Sérsic profile, the Petrosian (1976) photometry technique is applied, with the same parameters as used in the SDSS survey. This supplies seeing-corrected Petrosian magnitudes and radii. A K -corrected surface-brightness $\mu_{0.1i}$ in the $^{0.1}i$ band is computed by dividing half the K -corrected Petrosian light by the area of the Petrosian half-light circle.

For the purposes of computing large-scale structure statistics, we have assembled a complete subsample of SDSS galaxies known as the NYU LSS `sample12`. This subsample is described elsewhere (e.g., Blanton et al. 2003a); it is selected to have a well-defined window function and magnitude limit. In addition, the sample of galaxies used here was selected to have apparent magnitude in the range $14.5 < r < 17.77$ mag, redshift in the range $0.05 < z < 0.20$, and absolute magnitude $M_{0.1i} > -24$ mag. These cuts left 156,395 galaxies.

For each galaxy, a selection volume V_{\max} is computed, representing the total volume of the Universe (in h^{-3} Mpc 3) in which the galaxy could have resided and still made it into the sample. The calculation of these volumes is described elsewhere (Blanton et al. 2003b,a). For each galaxy, the quantity $1/V_{\max}$ is that galaxy's contribution to the cosmic number density, and the quantity L/V_{\max} , where L is the luminosity in some bandpass, is that galaxy's contribution to the luminosity density in that bandpass.

Around each galaxy in a complete subsample, `sample10`, of `sample12`, there is a measure of the overdensity δ_1 inside a spherical Gaussian window of radius $1 h^{-1}$ Mpc, made by deprojecting the angular distribution of nearby galaxies detected in the imaging at fluxes corresponding to luminosities within 1 mag of L^* at the target galaxy's redshift, as described elsewhere (Eisenstein 2003; Hogg et al. 2003). The individual overdensity estimates are low in signal-to-noise, but they are unbiased in the mean when averaged over sets of galaxies. A galaxy in an environment with the cosmic mean density has $\delta_1 = 0$.

There is another measure δ_8 on an $8 h^{-1}$ Mpc scale, that is a measure of the three-dimensional comoving number density excess around each galaxy in a sphere of $8 h^{-1}$ Mpc comoving radius, with no correction for peculiar velocities, as described elsewhere (Hogg et al. 2003; Blanton et al. 2003a). Neighbor galaxies are counted, the result is divided by the prediction made from the galaxy luminosity function (Blanton et al. 2003b), and unity is subtracted to produce the overdensity estimate. The estimates δ_8 are higher in signal-to-

noise than the estimates δ_1 , but they are slightly biased because they do not account for peculiar velocities.

3. Method

An average old stellar population spectrum (hereafter called “K” because it is dominated by K-type stars) was made by averaging the spectra of bulge-dominated galaxies with luminosities near L^* and in typical environments, as described previously (Eisenstein et al. 2003). An average A-star spectrum (“A”) was obtained by scaling and taking the mean of calibrated SDSS spectra of stars with types determined by eye to be near A0. These two spectra were normalized by scaling them to have equal total flux within the wavelength range $3800 < \lambda < 5400 \text{ \AA}$.

A linear sum of the K and A spectra was fit to every SDSS spectrum in the wavelength range $3800 < \lambda < 5400 \text{ \AA}$, weighting by the inverse square uncertainty in the observed spectrum. A 280 km s^{-1} region was masked out around $\text{H}\beta$ and the [O III] lines; this mask size was determined by observing that it would mask out the great majority of the emission-line flux in the great majority of spectra. Before fitting, the A spectrum was smoothed to the appropriate velocity dispersion for each spectrum. Dressler & Gunn (1983) pioneered this method by showing that post-starburst galaxies can be modeled well by an A dwarf spectrum and a K0 spectrum over the range of 3400 to 5400 angstroms. They found, as we do, that this model simultaneously describes the broad spectral continuum and the depths of narrow features.

The fitting procedure returns two numbers, the amplitudes K and A of the K and A spectral components in the best fit.

The $\text{H}\alpha$ line flux is measured in a 20 \AA width interval centered on the line. Before the flux is computed, the best-fit model A+K spectrum is scaled to have the same flux continuum as the data in the vicinity of the emission line and subtracted to leave a continuum-subtracted line spectrum. This method fairly accurately models the $\text{H}\alpha$ absorption trough in the continuum, although in detail it leaves small negative residuals, as will be shown below. The flux is converted to a rest-frame equivalent width (EW) with a continuum found by taking the inverse-variance-weighted average of two sections of the spectrum about 150 \AA in size and on either side of the emission line.

Some general caveats apply to our measurements. The first is that the K+A fit is not always good; in particular, galaxies that have undergone a very recent ($< 10^8 \text{ yr}$) starburst can have the blue end of their spectra dominated by O and B stars, not A stars. These

galaxies will be assigned high A/K , because the A template fits better than the K , even though the A stars are not dominating the spectra. Of course, most of these galaxies also show strong nebular $H\alpha$ emission, and, indeed, they do contain young stars.

We rely heavily on the flux-calibration of the spectra, because A/K is sensitive to the color or tilt of the spectrum. If there were large (> 20 percent) absolute calibration deviations among the galaxy spectra, we might introduce some spurious interlopers. However, the peak of the A/K distribution of galaxies with low $H\alpha$ EW at $A/K = 0$ is narrow and symmetrical about zero. This is a strong indicator that the spectrophotometric calibration is well-behaved. Note that we rely on the consistency of SDSS spectrophotometric calibration, but not on its absolute accuracy. The typical standard linear fitting errors in A/K are 0.03 to 0.1, roughly consistent with the scatter around $A/K = 0$.

We are looking at fiber spectra, inside the central 3 arcsec diameter of each galaxy. The physical size of this aperture is between 2 and $7 h^{-1}$ kpc in diameter, thereby excluding light from the outer parts of the galaxies. Some of our galaxies classified as $K+A$ could, in principle, have active star formation in their outskirts. Strictly speaking, the $K+A$ classification is a classification of the star formation indicators in the inner regions of galaxies. For this reason, in what follows the SDSS imaging rather than spectroscopy is used to measure global properties of the galaxies.

The fitting procedure doesn't take dust extinction into account. The A/K ratio is sensitive to the shape of the blue end of the spectrum, so it will be reduced in a galaxy in which the A stars are behind significant amounts of dust. This is also true of the $H\alpha$ EW measurements, although less so because $H\alpha$ is redward of the $K+A$ fitting region. For these reasons, there may be some truly post-starburst galaxies not classified as $K+A$ galaxies because their young stars are dust-enshrouded.

The $K+A$ population defined by this project does not contain any significant AGN because the selection permits so little $H\alpha$ emission. There may be some truly post-starburst galaxies not classified as $K+A$ galaxies because they contain central AGN and therefore emit significant $H\alpha$ emission.

4. Model spectra

The K , A , and $H\alpha$ measurements were made also on model spectra made by convolving PEGASE (Fioc & Rocca-Volmerange 1997) instantaneous starburst models with different star formation histories.

The original instantaneous starburst history was made with solar metallicity. Although nebular emission is included in the model, there was no modeling of galactic winds, infall, or internal extinction. For each timestep, the K and A measurements were computed with exactly the same least-square-fitting procedure as was performed on the data. The continuum around the $H\alpha$ line was also computed in exactly the same way as in the data, but the flux of the $H\alpha$ line was taken directly from the PEGASE outputs, because PEGASE returns integrated flux values for the emission lines rather than flux densities.

Three model spectra and associated evolutionary tracks were computed by convolving the instantaneous PEGASE burst model: A galaxy forming stars at a fixed rate for 14 Gyr; a galaxy forming stars at a fixed rate for 10 Gyr, shutting off, and fading quiescently for 4 Gyr; and a galaxy forming stars at a fixed rate for 3 Gyr, shutting off, and fading quiescently for 11 Gyr.

In the end, because of small differences between the old model spectra and old observed galaxies, the final K and A values were transformed (by a linear transformation equivalent to a flux-conserving shear in the K vs. A plane) so that an old model galaxy shows $A/K = 0$, just like an old real galaxy. The linear transformation affects the model outputs by less than 15 percent.

The measurements A/K and $H\alpha EW$ are plotted as a function of cosmic time for the three models in Figure 2.

5. Results

The measured A/K values for the galaxies in the sample are plotted against the measured $H\alpha EW$ values in Figure 3. The two star-formation indicators are highly correlated, as expected. Overplotted on the figure are models of galaxies with star formation histories consisting of constant star-formation rates followed by periods of total quiescence.

It is worthy of note that most of the galaxies appear more quiescent (i.e., have lower A/K and lower $H\alpha EW$) than the model (labeled “14”) in which stars form at a constant rate over the entire lifetime of the Universe. In other words, the present-day star-formation rate appears much lower than the cosmic time-averaged mean.

The models in which star formation has “shut off” drop precipitously in $H\alpha EW$ (which indicates stars with lifetimes of $\sim 10^7$ yr) and then slowly in A/K (which indicates stars with lifetimes of $\sim 10^9$ yr. The models suggest that galaxies whose star-formation activities have shut off will evolve into the zero-star-formation population along the zero $H\alpha EW$ line.

Indeed, Figure 3 shows a clear “spur” of galaxies along this line. These are the “K+A galaxies”.

Figure 4 shows the ratio of $H\alpha EW$ to A/K for samples cut in A/K . The histograms are bimodal, showing a population with anomalously low $H\alpha EW$. These are the K+A galaxies. The figure shows that K+A galaxies form an identifiable separate population. This figure also suggests that the line that separates the “K+A galaxies” from the rest of the population has a slope of $(H\alpha EW)/(A/K) = 5$ on Figure 3. This figure also shows that by defining “K+A galaxies” to have $A/K > 0.2$ we are excluding a large number of transition objects. The cut was put at 0.2 to avoid interlopers with true values of $A/K \approx 0.0$ but scattered high by calibration or statistical errors.

The selection of K+A galaxies for what follows is indicated by the green lines on Figure 3. There are 1194 K+A galaxies within these selection boundaries in `sample12`. Spectra of a randomly selected subsample of this population is shown in Figure 5.

The astute reader will notice that the mode $H\alpha EW$ is less than zero; this offset is due to the crudeness of the continuum model subtracted during $H\alpha$ line measurement. This offset does not affect any of our conclusions.

It is interesting to compare our selection criteria with those of Zabludoff et al. (1996) and Goto et al. (2003). Zabludoff et al. (1996) considered galaxies in the redshift range $0.05 < z < 0.13$ with [O II] emission $EW < 2.5$ Å and $H\gamma$, $H\delta$, and $H\beta$ absorption $EW > 5.5$ Å. They found 21 K+A galaxies out of a sample of 11113 (roughly 0.2 percent). Goto et al. (2003) also worked with an SDSS sample of galaxies, but in the redshift range $0.05 < z < 1.0$ and with $H\delta > 4$ Å. They found 3340 HDS galaxies out of a sample of 95479 (roughly 3.4 percent).

Figure 6 shows the luminosity function of the K+A galaxies compared with the luminosity function of the entirety of `sample12`. The shapes are very similar. Interestingly, the shape of the K+A luminosity function appears closer to the shape of the total luminosity function than it does to the early-type galaxy or red galaxy luminosity functions (e.g., Blanton et al. 2003b). In detail, quantitative comparisons of the luminosity functions ought to involve the fading with time of the K+A galaxy light.

Figure 7 shows the distribution of A/K for the K+A galaxies, in number-density units (the “ratio function”?). Overplotted are the expected distributions of A/K under the assumption of steady-state creation of K+A galaxies along evolutionary tracks like those of the “10” model (i.e., 10 Gyr of constant star formation followed by nothing) or the “3” model (i.e., 3 Gyr of constant star formation followed by nothing). Neither of these models is a good description, suggesting that there is probably a large diversity to the star-formation histories that end in a K+A phase according to the selection criteria used here.

Figure 8 shows the luminosity-density weighted distribution of all galaxies in the plane of $0.1(g - r)$ color and Sérsic index n (seeing-corrected concentration). As discussed elsewhere (Blanton et al. 2003a), the general galaxy population is bimodal in this plane, showing a population of blue, exponential (disk-dominated) galaxies and a separate population of red, concentrated (bulge-dominated) galaxies. Figure 8 also shows that galaxies chosen to have high star-formation rates, by either A/K or $H\alpha EW$, lie predominantly in the blue, exponential class. Galaxies chosen to have low star-formation rates lie predominantly in the red, concentrated class. Galaxies chosen to have high A/K but low $H\alpha EW$ —the $K+A$ galaxies—have some members clearly in the blue, exponential class, and some in an outlier class that appears concentrated, but blue. If star formation has truly been shut off in these galaxies, they are expected to fade and redden and become part of the red, concentrated class.

Figure 9 is similar to Figure 8 but shows the distribution of objects in the color-surface-brightness plane. The population of objects in this plane is not clearly bimodal, however the bulge-dominated galaxies form a strong peak at high surface brightnesses and red colors. Just like Figure 8, this shows that galaxies with high A/K or high $H\alpha EW$ appear to be disk-dominated and galaxies with low A/K or low $H\alpha EW$ appear to be bulge-dominated. The $A+K$ population shows even higher surface brightnesses than the bulge-dominated galaxies, suggesting that as they age, the $A+K$ galaxies will fade and redden into the bulge-dominated part of the diagram.

Three-color images made from the SDSS imaging were inspected by eye for a randomly selected sample of 160 of the $K+A$ galaxies in the sample. The vast majority of them (~ 90 percent) appear bulge dominated. The ~ 10 percent that appear to be disk dominated do also show significant bulges. About 30 percent either show tidal features or lie extremely close on the sky to nearby neighbors, indicating possible past or current interactions.

In Table 1, the mean overdensities $\langle \delta_1 \rangle$ and $\langle \delta_8 \rangle$ on the $1 h^{-1}$ and $8 h^{-1}$ Mpc scales are given for the different galaxy populations mentioned above. Error bars on these averages were computed by splitting the sample into three disjoint sky regions. This technique produces conservative error estimates because it effectively includes contributions from variations in calibration and large-scale structure. The numbers of galaxies used for mean overdensities are smaller than used in the Figures because overdensities have only been calculated on an unbiased subsample of the sample we are using. Table 1 shows that $K+A$ galaxies, on average, live in the lower-density regions more typical of spiral galaxies, and not the higher-density regions typical of bulge-dominated galaxies.

6. Discussion

Two star-formation indicators, $H\alpha$ EW and A/K , with two different timescales, $\sim 10^7$ yr and $\sim 10^9$ yr, have been measured in a sample of 156,395 SDSS (optically selected) galaxies in the redshift range $0.05 < z < 0.20$. The two star-formation indicators are strongly correlated, as expected. Comparison with models shows that the average levels of star formation in these galaxies is below the average over cosmic time. This fits in with many observations of more distant galaxies that have implied a rapid decrease in the global comoving star formation rate with cosmic time to the present day (Hogg 2001, and references therein).

A clearly separated, distinct population of “K+A galaxies” is found, with very weak or no $H\alpha$ EW, but significant A/K . The star-formation indicators $H\alpha$ EW and A/K have very different timescales over which, in effect, they average recent star formation rates. Galaxies that abruptly (ie, on timescales $< 10^9$ yr) shut off star formation will fade rapidly in $H\alpha$ EW, but slowly in A/K . This timescale mismatch explains the presence of the distinctly visible K+A population shown in Figure 3; we expect these galaxies to indicate abruptly terminated star formation.

Bulge-dominated and disk-dominated galaxies can be separated by their colors, concentrations (Sérsic indices), and surface brightnesses. By these measures, most of the K+A galaxies appear to be bluer, higher surface-brightness counterparts of bulge-dominated galaxies. The offsets in color and surface brightness are consistent with the fading and redenning expected in the evolution of stellar populations. Taken on face value, this is evidence that K+A galaxies are plausibly the post-starburst progenitors of typical bulge-dominated galaxies, as might be expected in a scenario in which disk-dominated galaxies, for instance, merge to form bulge-dominated galaxies.

Interestingly, if that conclusion is correct, then these K+A galaxies are the progenitors of the bulge-dominated galaxies of the field, not of rich clusters, because the K+A galaxies live in the typical overdensities of spirals, not ellipticals. Past work on K+A galaxies has implied that they form a special cluster population (eg, Dressler & Gunn 1983), but this is presumably a consequence of the selection in those studies.

In order to put the steady-state predictions onto Figure 7, it was necessary to multiply the time spent at each value of A/K , or $|dt/d(A/K)|$ by a comoving rate density to match the total abundance. This rate density is 1.8 or 1.0 times $10^{-4} h^3 \text{ Mpc}^{-3} \text{ Gyr}^{-1}$ for the “3” or “10” model respectively. In other words, the comoving K+A galaxy creation rate density is on this order at redshifts $z \sim 0.1$. This suggests that of order 1 percent of galaxies are currently K+A, and of order 10 percent have been through a K+A phase since redshift unity.

The A and K spectra used for this study will be made available with the electronically

published version of this article.

We thank Douglas Finkbeiner, Michel Fioc, Robert Lupton, Bob Nichol, Jim Peebles, Don Schneider, David Spergel, Michael Strauss, and Christy Tremonti for useful ideas, conversations, and software. This research made use of the NASA Astrophysics Data System. ADQ, DWH, and MRB are partially supported by NASA (grant NAG5-11669) and NSF (grant PHY-0101738). DJE is supported by NSF (grant AST-0098577) and by an Alfred P. Sloan Research Fellowship.

Funding for the creation and distribution of the SDSS Archive has been provided by the Alfred P. Sloan Foundation, the Participating Institutions, the National Aeronautics and Space Administration, the National Science Foundation, the U.S. Department of Energy, the Japanese Monbukagakusho, and the Max Planck Society. The SDSS Web site is <http://www.sdss.org/>.

The SDSS is managed by the Astrophysical Research Consortium for the Participating Institutions. The Participating Institutions are The University of Chicago, Fermilab, the Institute for Advanced Study, the Japan Participation Group, The Johns Hopkins University, Los Alamos National Laboratory, the Max-Planck-Institute for Astronomy, the Max-Planck-Institute for Astrophysics, New Mexico State University, University of Pittsburgh, Princeton University, the United States Naval Observatory, and the University of Washington.

REFERENCES

Barry, D. C. 1988, *ApJ*, 334, 436

Blanton, M. R., Brinkmann, J., Csabai, I., Doi, M., Eisenstein, D. J., Fukugita, M., Gunn, J. E., Hogg, D. W., & Schlegel, D. J. 2003, *AJ*, 125, 2348

Blanton, M. R., Lin, H., Lupton, R. H., Maley, F. M., Young, N., Zehavi, I., & Loveday, J. 2003, *AJ*, 125, 2276

Blanton, M. R. et al. 2003a, *ApJ*, in press (astro-ph/0209479)

Blanton, M. R. et al. 2003b, *ApJ*, in press (astro-ph/0210215)

Blitz, L. 1996, in IAU Symp. 170: CO: Twenty-Five Years of Millimeter-Wave Spectroscopy, 11–18

Chang, T., van Gorkom, J. H., Zabludoff, A. I., Zaritsky, D., & Mihos, J. C. 2001, *AJ*, 121, 1965

Dressler, A. & Gunn, J. E. 1983, *ApJ*, 270, 7

Eisenstein, D. J. 2003, *ApJ*, 586, 718

Eisenstein, D. J. et al. 2001, *AJ*, 122, 2267

Eisenstein, D. J. et al. 2003, *ApJ*, 585, 694

Fioc, M. & Rocca-Volmerange, B. 1997, *A&A*, 326, 950

Fukugita, M., Hogan, C. J., & Peebles, P. J. E. 1998, *ApJ*, 503, 518

Fukugita, M., Ichikawa, T., Gunn, J. E., Doi, M., Shimasaku, K., & Schneider, D. P. 1996, *AJ*, 111, 1748

Gizis, J. E., Reid, I. N., & Hawley, S. L. 2002, *AJ*, 123, 3356

Goto, T. et al. 2003, *PASJ*, submitted (astro-ph/0301305)

Gunn, J. E., Carr, M. A., Rockosi, C. M., Sekiguchi, M., et al. 1998, *AJ*, 116, 3040

Hogg, D. W. 1999, astro-ph/9905116

Hogg, D. W. 2001, astro-ph/0105280

Hogg, D. W., Blanton, M. R., Eisenstein, D. J., Gunn, J. E., Schlegel, D. J., Zehavi, I., Bahcall, N. A., Brinkmann, J., Csabai, I., Schneider, D. P., Weinberg, D. H., & York, D. G. 2003, *ApJ*, 585, L5

Hogg, D. W. et al. 2002, *AJ*, 124, 646

Kennicutt, R. C., Tamblyn, P., & Congdon, C. E. 1994, *ApJ*, 435, 22

Lupton, R. H., Gunn, J. E., Ivezić, Z., Knapp, G. R., Kent, S., & Yasuda, N. 2001, in ASP Conf. Ser. 238: Astronomical Data Analysis Software and Systems X, Vol. 10, 269–??

Mooney, T. J. & Solomon, P. M. 1988, *ApJ*, 334, L51

Norton, S. A., Gebhardt, K., Zabludoff, A. I., & Zaritsky, D. 2001, *ApJ*, 557, 150

Pardi, M. C. & Ferrini, F. 1994, *ApJ*, 421, 491

Petrosian, V. 1976, *ApJ*, 209, L1

Pier, J. R., Munn, J. A., Hindsley, R. B., Hennessy, G. S., Kent, S. M., Lupton, R. H., & Ivezić, Ž. 2003, *AJ*, 125, 1559

Prantzos, N. & Silk, J. 1998, *ApJ*, 507, 229

Prugniel, P. & Soubiran, C. 2001, *A&A*, 369, 1048

Richards, G. et al. 2002, *AJ*, 123, 2945

Roberts, M. S. & Haynes, M. P. 1994, *ARA&A*, 32, 115

Rocha-Pinto, H. J., Scalo, J., Maciel, W. J., & Flynn, C. 2000, *A&A*, 358, 869

Schlegel, D. J., Finkbeiner, D. P., & Davis, M. 1998, *ApJ*, 500, 525

Smith, J. A., Tucker, D. L., et al. 2002, *AJ*, 123, 2121

Stoughton, C. et al. 2002, *AJ*, 123, 485

Strauss, M. A. et al. 2002, *AJ*, 124, 1810

Worthey, G. 1998, *PASP*, 110, 888

York, D. et al. 2000, *AJ*, 120, 1579

Zabludoff, A. I., Zaritsky, D., Lin, H., Tucker, D., Hashimoto, Y., Shectman, S. A., Oemler, A., & Kirshner, R. P. 1996, *ApJ*, 466, 104

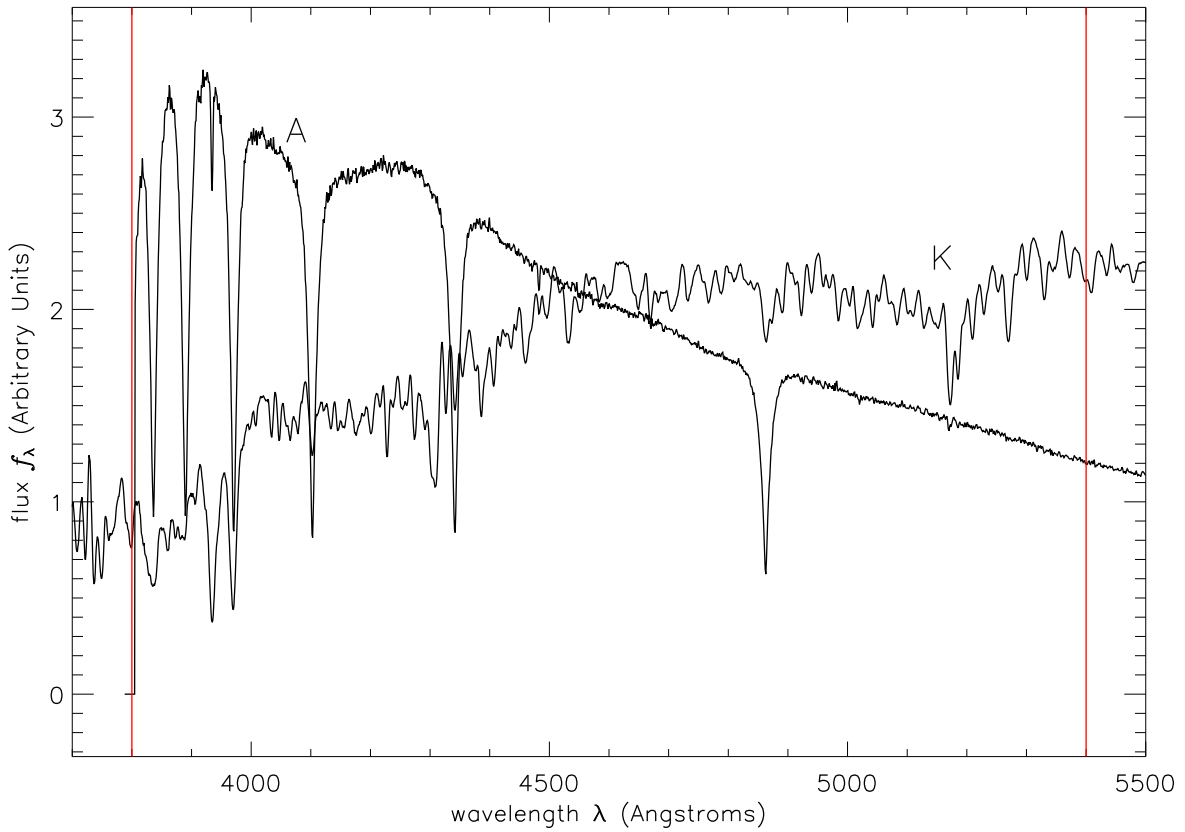


Fig. 1.— The normalized model A-star spectrum (“A”) and average old stellar population spectrum (“K”) used in the K+A fits. The vertical lines indicate the region over which the fit was performed. As stated in the text, the spectra have equal areas inside the fitting region.

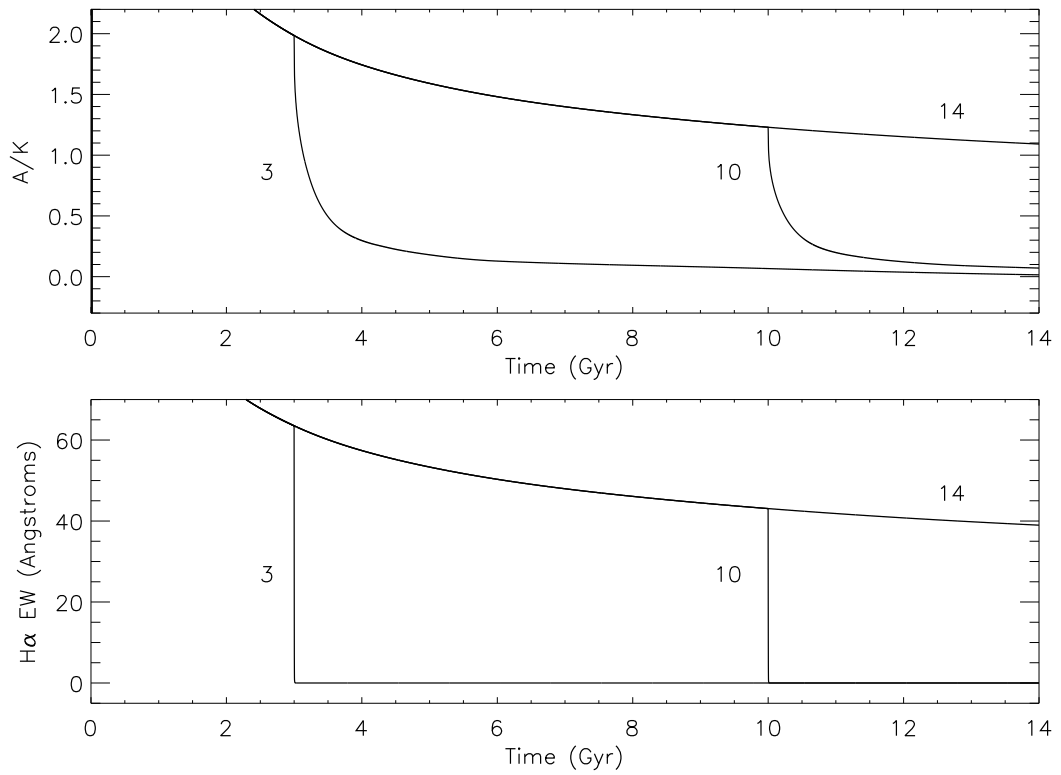


Fig. 2.— The indicators A/K and $H\alpha$ plotted against time for the three star formation models with constant star formation for 14, 10, and 3 Gyr, followed by quiescent fading (see text for details).

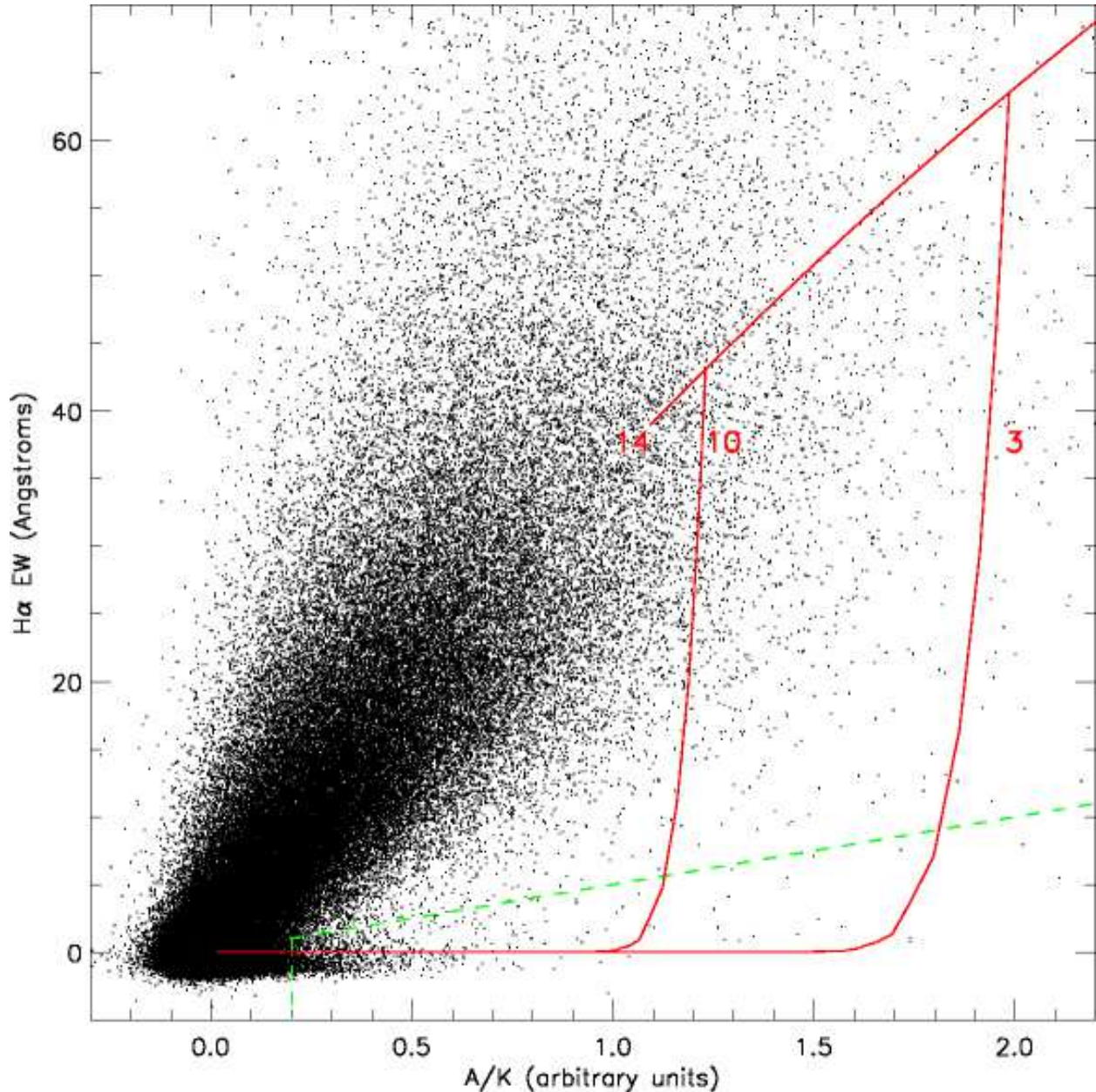


Fig. 3.— The distribution of A/K vs $H\alpha$ for all the galaxies in this sample. Typical errors in A/K are ~ 0.03 to 0.1 . Shown in red are model tracks for the 3 models shown in Figure 2. The K+A galaxy population was selected with the cuts shown in green.

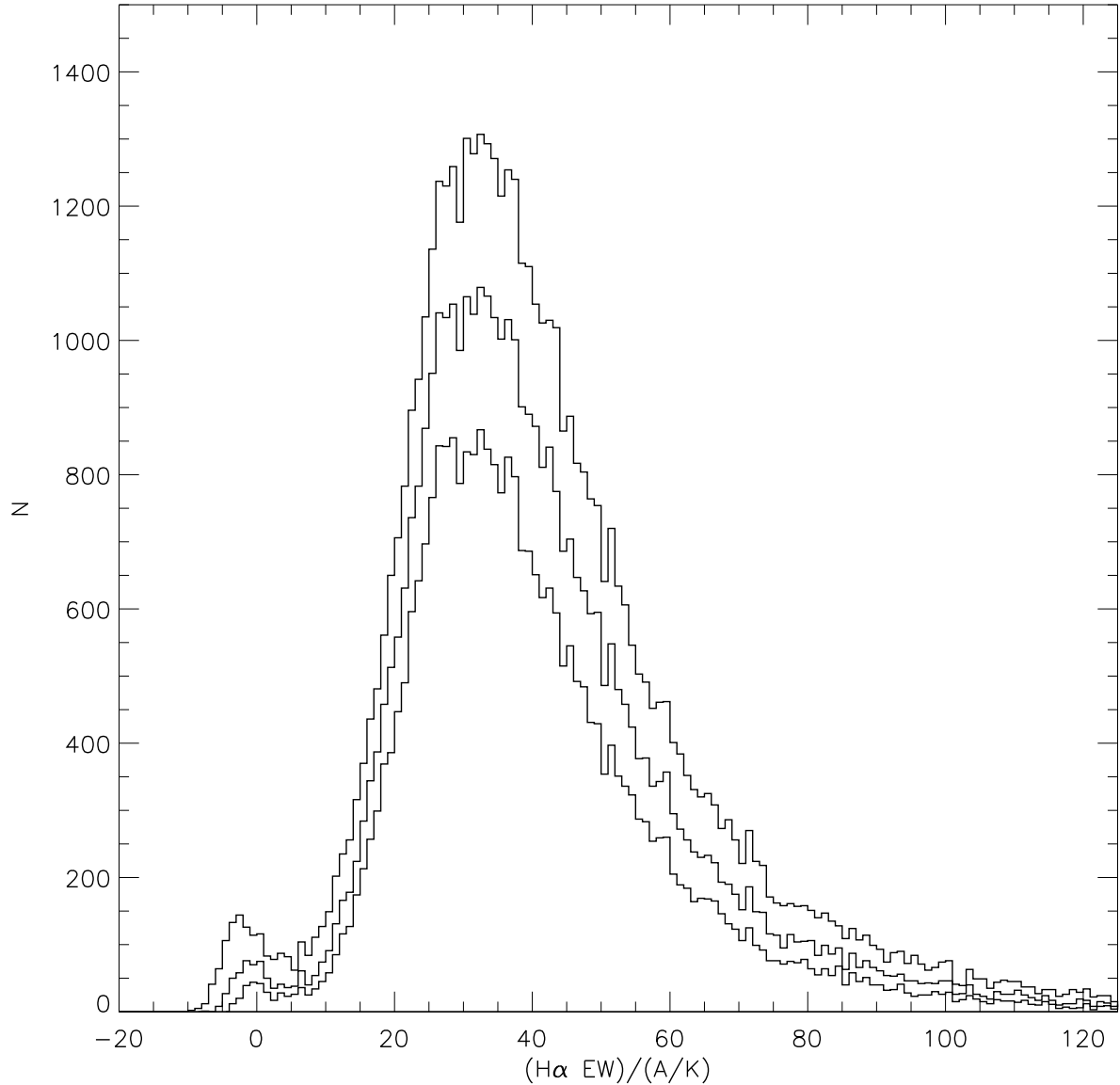


Fig. 4.— The distributions of the ratio of the two star formation indicators, $H\alpha$ EW and A/K , for four subsamples of `sample12`, selected to have $A/K > 0.2$, 0.3 , and 0.4 . Note the evidence for the existence of a separate population of K+A galaxies around zero.

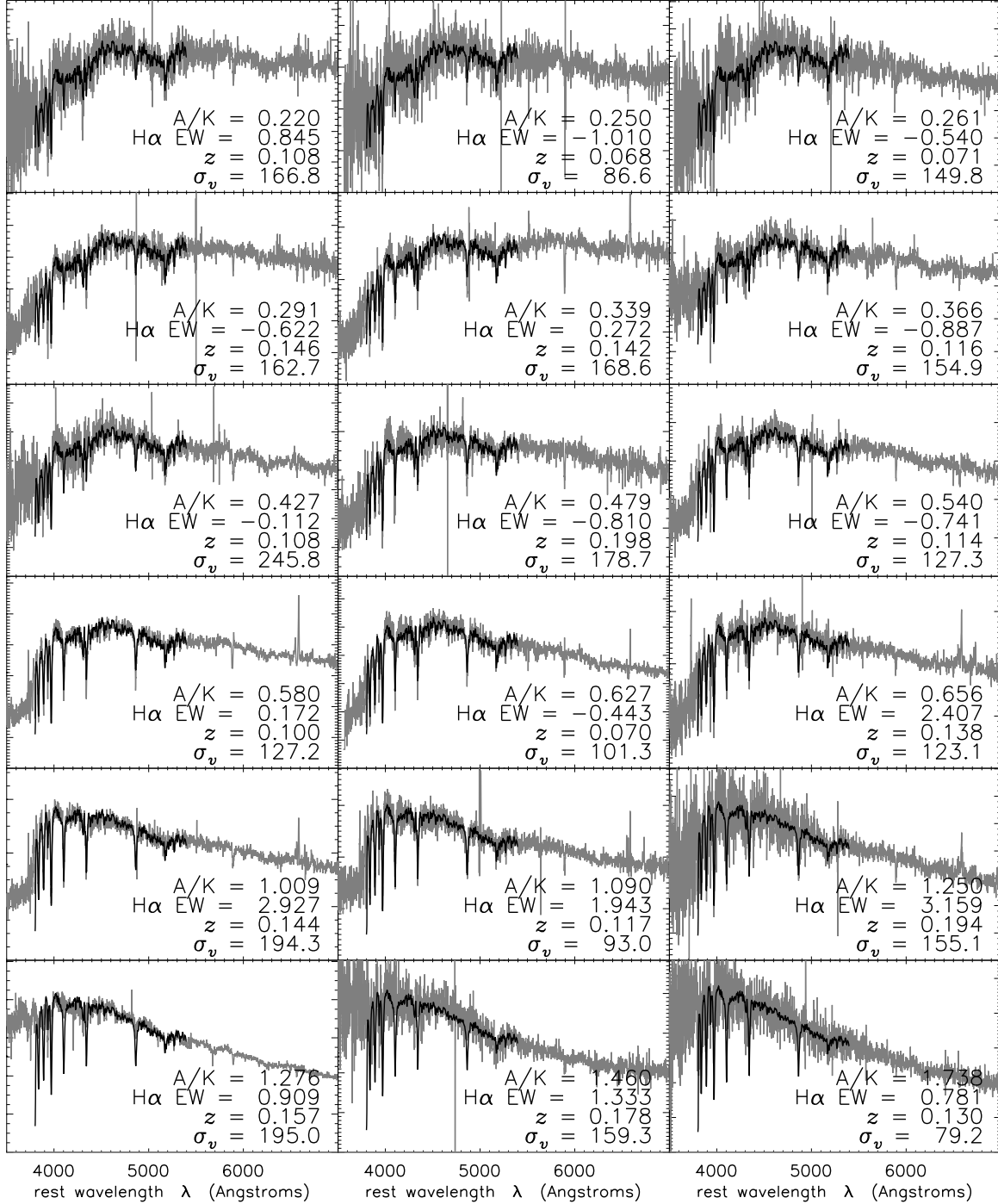


Fig. 5.— Spectra of members of a randomly selected subsample of the K+A population, selected from A/K bins so as to span the range. The grey lines show the data and the black overplotted lines show the “K+A” best fit.

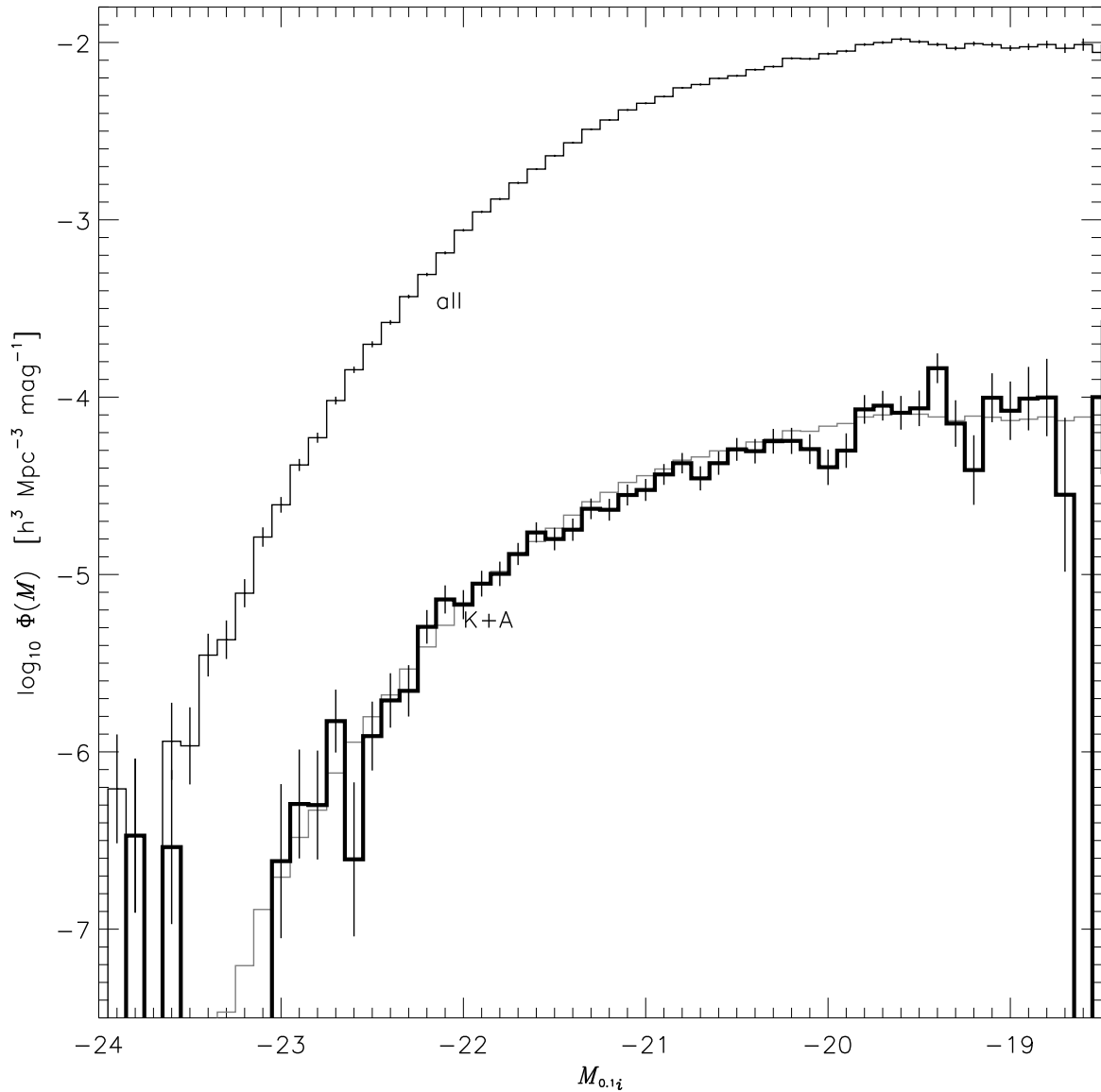


Fig. 6.— The luminosity function—i.e., luminosity distribution of the sample weighted by $1/V_{\max}$ —for the entire sample and the K+A galaxies. The plotted uncertainties are simply the $1/V_{\max}$ weights added in quadrature (divided by the bin width).

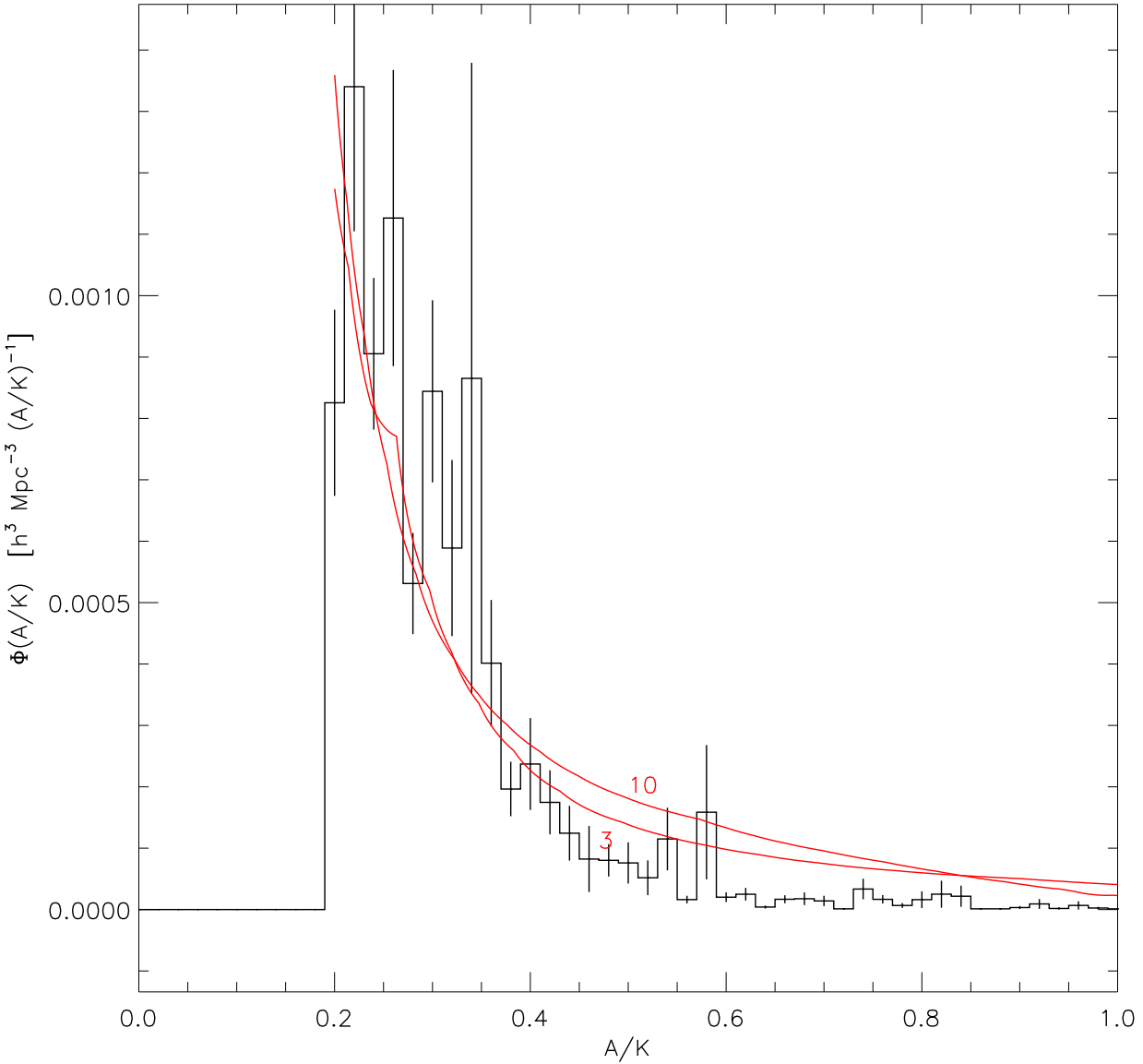


Fig. 7.— The distribution of A/K , weighted by $1/V_{\max}$, to make a “ratio function”. Overplotted are curves proportional to $|dt/d(A/K)|$ for the the “10” and “3” Gyr models of Figure 2. These curves are equivalent to “steady-state” predictions made under the assumptions that (a) all galaxies have the same star-formation history, and (b) galaxies are passing through the $A+K$ phase at a rate that varies slowly on Gyr timescales. The plotted uncertainties are simply the $1/V_{\max}$ weights added in quadrature (divided by the bin width).

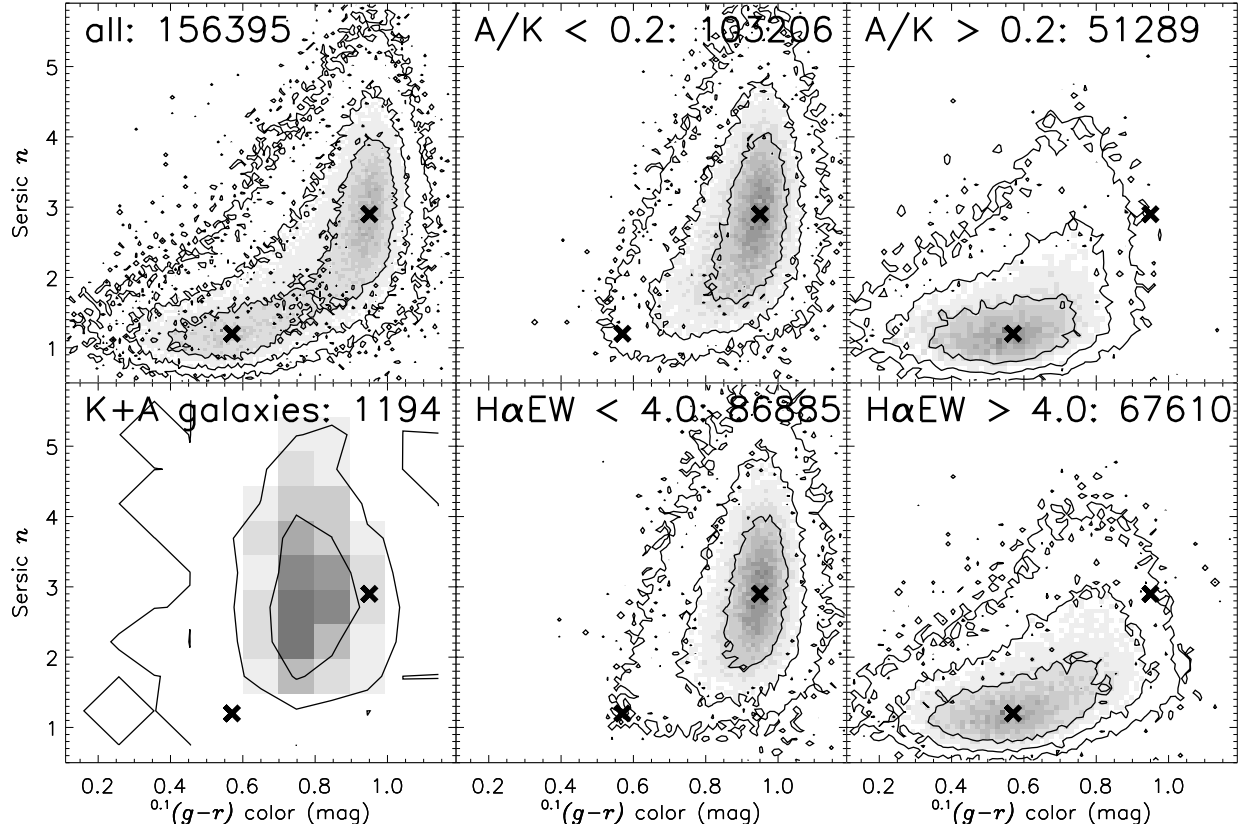


Fig. 8.— The top left panel shows the distribution of luminosity density in galaxies in the sample in the color–Sérsic-index plane. The color is measured in blueshifted SDSS band-passes $^{0.1}g$ and $^{0.1}r$, and the Sérsic index n is found by fitting to the radial profile in the $^{0.1}i$ band. Each galaxy data point has been weighted by the ratio of its luminosity $L_{0.1i}$ in the $^{0.1}i$ band to its comoving selection volume V_{\max} , so the distribution of weight in the plot is proportional to comoving luminosity density. The contours enclose 52.0, 84.3, and 96.6 percent of the total luminosity density. In this panel, galaxies separate into disk-dominated (blue, low n) and bulge-dominated (red, high n) populations, marked by crosses. The other panels show similar plots, but for different sub-samples, cut on A/K and $H\alpha EW$. The “K+A” panel shows those galaxies making the high A/K cut and the low $H\alpha EW$ cut. Galaxies selected to have low A/K or low $H\alpha EW$ appear to be concentrated (bulge-dominated); galaxies selected to have high A/K or high $H\alpha EW$ appear to be exponential (disk-dominated). The K+A galaxies have the colors of disk-dominated galaxies but many have the radial profiles of bulge-dominated galaxies.

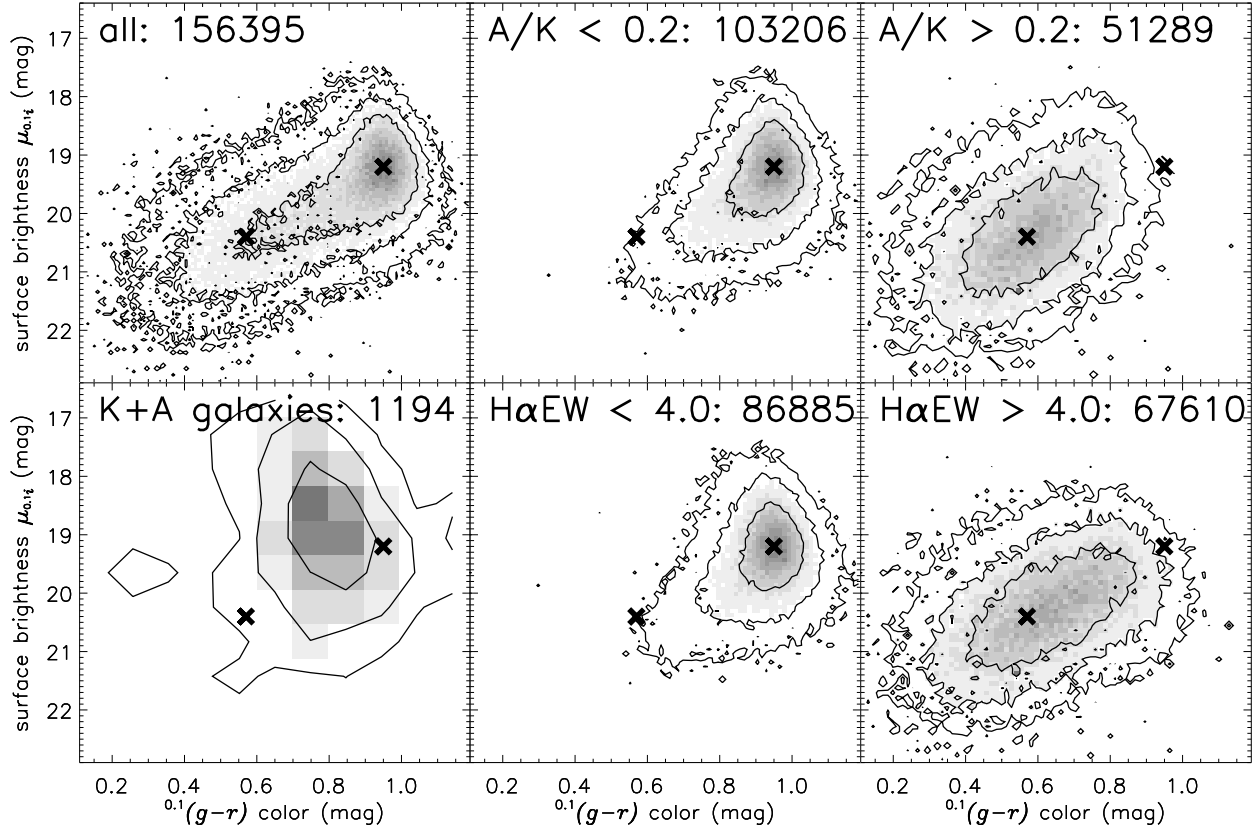


Fig. 9.— Similar to Figure 8 but showing the distribution of luminosity density in galaxies in the sample in the color–surface-brightness plane. For each galaxy, the surface brightness $\mu_{0,1i}$ is the mean surface brightness inside the Petrosian R_{50} radius of the best-fitting Sérsic radial profile in the $0.1i$ band. In this panel, again, galaxies also separate into disk-dominated (blue, low μ) and bulge-dominated (red, high μ) populations, marked by crosses. Galaxies selected to have low A/K or low H α EW appear to be high in surface brightness (bulge-dominated); galaxies selected to have high A/K or high H α EW appear to be lower in surface brightness (disk-dominated). The K+A galaxies have the colors of disk-dominated galaxies but many have central surface brightnesses as high as, or even higher than, bulge-dominated galaxies.

Table 1. average overdensities around galaxy subsamples

subsample	N	$j_{0.1i}/j_{\text{total}}$	^a	$\langle\delta_1\rangle$	$\langle\delta_8\rangle$
all	125255	1.000	19.8 ± 1.7	1.86 ± 0.19	
disk-dominated ($n < 2.0$)	49615	0.433 ± 0.007	13.7 ± 1.0	1.55 ± 0.19	
bulge-dominated ($n > 2.0$)	75640	0.567 ± 0.007	24.5 ± 2.2	2.10 ± 0.18	
K+A galaxies (see text)	1143	0.009 ± 0.001	15.0 ± 2.3	1.64 ± 0.20	

^aFraction of the total galaxy luminosity density in the $^{0.1}i$ band (i.e., total of $L_{0.1i}/V_{\text{max}}$) contributed by each subsample.